

Current Design with Minimum Error in Transcranial Direct Current Stimulation

Jing Qin^{1(⊠)}, Yushan Wang², and Wentai Liu²

Department of Mathematical Sciences, Montana State University,
Bozeman, MT, USA
jing.gin@montana.edu

Abstract. As a non-invasive brain stimulation technology, transcanial direct current stimulation (tDCS) has been recently attracting more and more attention in research and clinic applications due to its convenient implementation and modulation of the brain functionality. In this paper, we propose a novel multi-electrode tDCS current configuration model that minimizes the total error under the safety constraints. After rewriting the model as a linearly constrained minimization problem, we develop an efficient numerical algorithm based on the alternating direction method of multipliers (ADMM). Numerical experiments have shown the great potential of the proposed method in terms of accuracy and focality.

Keywords: transcranial Direct Current Stimulation (tDCS) Human head model · Multi-electrode stimulation · Safety constraints Alternating Direction Method of Multipliers (ADMM)

1 Introduction

Transcranial direct current stimulation (tDCS) is an emerging non-invasive brain stimulation technology that applies a small amount of direct currents on the electrodes placed on a human scalp surface to elicit modulation of neural activities [14]. It serves as an important therapeutic tool in clinics to treat psychiatric conditions and neurological diseases, including depression [3], Parkinson's disease [6], and epilepsy [1]. The tDCS modulates brain functions mainly through two ways. Firstly, it affects the neuronal activities directly by inducing the cortical changes. Secondly, it affects the neuronal network dynamics by either enhancing or hindering the synaptic transmission ability.

Although tDCS has a lot of practical advantages such as the portability, flexibility and tolerable stimulation duration, it faces several challenges such as the limited stimulation intensity and focality of detecting the stimulating electric field (e-field). To address these issues, many optimization based methods have

© Springer Nature Switzerland AG 2018

S. Wang et al. (Eds.): BI 2018, LNAI 11309, pp. 52-62, 2018.

² Department of Bioengineering, University of California, Los Angeles, CA, USA {yushanwang,wentai}@ucla.edu

been developed in the past. In particular, least squares methods are proposed to design the configuration of electrodes to minimize a second-order error [5]. In addition, several constraints are considered, including the maximum allowable value for the intensity for each electrode and the current sum due to the safety regulations, and the zero net current flow according to the reservation law. Similar to the beamforming problem, the linearly constrained minimum variance (LCMV) method is proposed in [5] to minimize the total power while utilizing the remaining degrees of freedom. However, LCMV suffers several drawbacks. Firstly, since minimization of the ℓ_2 -norm leads to a result with uniformly distributed errors, there is no guarantee that the resulting electric field exhibits a maximum at the target. Then an undesired cortex region may be stimulated in the LCMV results. Lastly, it causes the high possibility to get an empty solution set. One can also see that if the current intensity is smaller in the target regions, then the reconstructed electrodes are more focalized. Recently, weighted least squares methods are proposed to improve the accuracy, such as Minimize the Error Relative to No Intervention (ERNI) [12]. To maximize the intensity along a desired direction at the target region, a linear objective function that describes the projected intensity is also used [9,13].

Besides, errors with unknown statistics occur inevitably due to the signal transmission in tDCS. In the signal/image processing community, it is well known that the ℓ_1 -norm data fidelity is more robust to various noise/error types than its ℓ_2 -norm counterpart [4,10]. Different from ℓ_2 -norm minimization resulting in uniform error distribution, minimization of the ℓ_1 -norm of the error vector leads to a sparse solution with nonuniform error distribution. In the pursuit of high electrode focality, we propose a ℓ_1 -norm fidelity based model with the three commonly used constraints due to the safety regulation. By expressing the constraints using the indicator functions, we are able to convert the proposed nonlinear constrained minimization problem into a linear constrained one. Based on the alternating direction method of multipliers (ADMM), we derive an efficient numerical algorithm to solve the proposed model. In particular, each subproblem in the algorithm has a closed-form solution which brings computational convenience. Numerical experiments on multiple data sets have shown the proposed effectiveness and flexibility in achieving the ideal current configuration.

The rest of the paper is organized as follows. Section 2 describes the proposed mathematical model for the optimal configuration of tDCS electrode currents. To solve this minimization problem with linear constraints, we derive an efficient numerical algorithm base on ADMM. In Sect. 3, two sets of simulation experiments are conducted to verify the effectiveness of the proposed method. Finally, we draw conclusions and discuss future works in Sect. 4.

2 Methods

2.1 Simulation of a Realistic Head Model

The computational realistic head model utilized in our study is the anatomical template from Fieldtrip [11], which is derived from the Statistical Parametric

Mapping (SPM) Canonical Brain. The model contains essential parts in our study, including scalp, skull, cerebrospinal fluid (CSF), and the cortex. The boundaries of all the tissue layers of the model were first saved in stereolithography (STL) format, and then converted to the solid models using SolidWorks https://www.solidworks.com/. In addition, we also constructed 342-electrode system for the head model, the location of which is based on the international electroencephalography (EEG) system. The electrodes consist of the metal layer and the gel layer, where the gel layer lays between the metal and scalp as the real clinical application. Both of the layers have the same diameter of 6 mm and thickness of 1 mm. Figure 1 shows the head model and the distribution of electrodes.

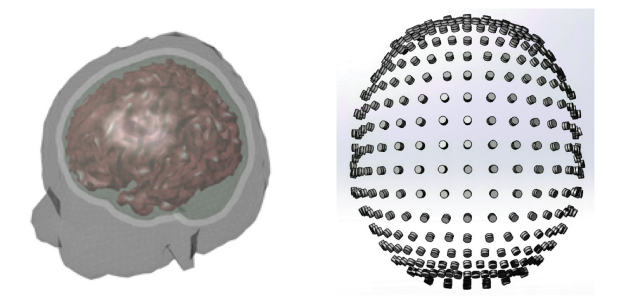


Fig. 1. Illustration of the head model and the electrode distribution.

Under the quasi-static condition, the injected current at each electrode has a linear relationship with the e-field value in each voxel, which is exactly the single element of the lead field matrix. Using FEM and solving Laplace equation in the realistic head model, we obtain one column by assigning a unit current (1mA) to that corresponding electrode and then complete the lead field matrix by repeating 342 times. All the simulation work is done by COMSOL Multiphysics 5.2 https://www.comsol.com/.

2.2 Proposed Mathematical Model

Let m be the number of voxels, n the number of electrodes, $\mathbf{s} \in \mathbb{R}^n$ the electrode current, \mathbf{e}_d the desired e-field distribution of the cortex, \mathbf{e}_0 the desired electric field distribution of the target region, and $K \in \mathbb{R}^{m \times n}$ be the lead field matrix. In general, the desired electric field \mathbf{e}_d and the electrode current \mathbf{s} are linearly related through $K\mathbf{s} = \mathbf{e}_d + \varepsilon$ where $\varepsilon \in \mathbb{R}^m$ is an error term. Denote I_{max} the maximal direct current and I_{total} the total currents injected into the head. Due to the safety regulations, the magnitude of each electrode current can not exceed I_{max} , and the sum of all currents in magnitude should be no more than $2I_{total}$. In addition, the conservation law of currents requires that the sum of all currents is zero. By taking all factors into consideration, we define the following feasible set

$$S = \{ \mathbf{s} \in \mathbb{R}^n : |s_i| \le I_{\text{max}}, \quad \sum_{i=1}^n |s_i| \le 2I_{total}, \quad \sum_{i=1}^n s_i = 0 \}.$$
 (1)

Next we introduce the ℓ_{∞} -norm and the ℓ_1 -norm of a vector, i.e., $\|\mathbf{x}\|_{\infty} = \max_{1 \leq i \leq n} |x_i|$ and $\|\mathbf{x}\|_1 = \sum_{i=1}^n |x_i|$ for any $\mathbf{x} \in \mathbb{R}^n$. Using the vector norms, we can get an equivalent form of (1)

$$S = \{ \mathbf{s} \in \mathbb{R}^n : \|\mathbf{s}\|_{\infty} \le I_{\text{max}}, \quad \|\mathbf{s}\|_1 \le 2I_{total}, \quad \mathbf{s}^T \mathbf{1} = 0 \},$$
 (2)

where $\mathbf{1} = (1, \dots, 1)^T \in \mathbb{R}^n$. From the practical perspective, we wish that the generated electric field can reach the desired value at the target region while small errors are allowed at the other regions, which causes the error vector ε to be sparse. To enhance the sparsity of ε and allow a nonuniform distribution of errors, we propose the following model that minimizes the total error

$$\min_{\mathbf{s} \in S} ||K\mathbf{s} - \mathbf{e}_d||_1. \tag{3}$$

Notice that the objective function in this problem is convex and non-differentiable but not strongly convex as the widely used total error power or its weighted variants [5], i.e., $||W(K\mathbf{s} - \mathbf{e}_d)||_2^2$ with the matrix of weights W. To handle this non-differentiability, we first convert (3) into a linearly constrained problem, and then resort to ADMM which can split multiple operators in the objective function and involve the fast proximal operator of the ℓ_1 -norm.

2.3 Proposed Numerical Algorithm

In this section, we propose an efficient algorithm to solve (3). Recently, ADMM has become one of the most popular optimization methods with guaranteed convergence in a variety of application problems [2,7,8]. Given a convex linear constrained minimization problem whose objective function consists of multiple separable terms, ADMM aims to split the entire problem into several subproblems and alternate updating variables iteratively. At each iteration, each subproblem can either have a closed-form solution or be solved efficiently. However, ADMM introduces multiple auxiliary variables corresponding to the linear constraints. To reduce the number of auxiliary variables, we first express the solution variable using the linear constraint in S. It is worth noting that maintaining this linear constraint will induce one additional auxiliary variable and one more penalty in the augmented Lagrangian function which causes slightly slower convergence. Since $\mathbf{s}^T \mathbf{1} = 0$, i.e., $\mathbf{1}^T \mathbf{s} = 0$, we can deduce that \mathbf{s} is in the nullspace of $\mathbf{1}^T$, denoted by $\mathcal{N}(\mathbf{1}^T)$. Let $B \in \mathbb{R}^{n \times (n-1)}$ be a null-space basis matrix of $\mathbf{1}^T$, i.e., the range of B satisfies $\mathcal{R}(B) = \mathcal{N}(\mathbf{1}^T)$. Then the rank-nullity theorem yields that there exists $\mathbf{x} \in \mathbb{R}^{n-1}$ such that $\mathbf{s} = B\mathbf{x}$. For example, we can choose

$$B = \begin{bmatrix} 1 & 1 & \cdots & 1 \\ -1 & 0 & \cdots & 0 \\ & \ddots & \ddots & \\ 0 & 0 & \cdots & -1 \end{bmatrix}_{n \times (n-1)}.$$

One can see that the columns of B form a basis of $\mathcal{N}(\mathbf{1}^T)$. By introducing the null-space basis matrix B of $\mathbf{1}^T$, the proposed model (3) turns into

$$\min_{\substack{\mathbf{s} \in C_1, \mathbf{z} \in C_2 \\ \mathbf{x}, \mathbf{y} \in \mathbb{R}^n}} \|\mathbf{y}\|_1, \quad \text{s.t.} \quad \mathbf{s} = B\mathbf{x}, \, \mathbf{y} = K\mathbf{s} - \mathbf{e}_d, \, \mathbf{z} = \mathbf{s}.$$
 (4)

Here C_1 and C_2 are convex sets which are defined to be $C_1 = \{\mathbf{s} \in \mathbb{R}^n : \|\mathbf{s}\|_{\infty} \le I_{\max}\}$ and $C_2 = \{\mathbf{z} \in \mathbb{R}^n : \|\mathbf{z}\|_1 \le 2I_{total}\}$, respectively. Next we define an augmented Lagrangian function

$$\mathcal{L}(\mathbf{s}, \mathbf{x}, \mathbf{y}, \mathbf{z}, \widehat{\mathbf{x}}, \widehat{\mathbf{y}}, \widehat{\mathbf{z}}) = \|\mathbf{y}\|_1 + \frac{\rho_1}{2} \|\mathbf{s} - B\mathbf{x} + \widehat{\mathbf{x}}\|_2^2 + \frac{\rho_2}{2} \|\mathbf{y} - K\mathbf{s} + \mathbf{e}_d + \widehat{\mathbf{y}}\|_2^2 + \frac{\rho_3}{2} \|\mathbf{z} - \mathbf{s} + \widehat{\mathbf{z}}\|_2^2 + \iota_{C_1}(\mathbf{s}) + \iota_{C_2}(\mathbf{z}).$$

Here ι_{Ω} is the indicator function defined by $\iota_{\Omega}(\mathbf{x}) = 0$ if $\mathbf{x} \in \Omega$ and ∞ otherwise. Note that $\mathbf{x} \in \mathbb{R}^{n-1}$, $\hat{\mathbf{x}}, \mathbf{s}, \mathbf{z}, \hat{\mathbf{z}} \in \mathbb{R}^n$, $\mathbf{y}, \hat{\mathbf{y}}, \mathbf{e}_d \in \mathbb{R}^m$, $B \in \mathbb{R}^{n \times (n-1)}$ and $K \in \mathbb{R}^{m \times n}$.

We first group the two sets of variables $(\mathbf{x}, \mathbf{y}, \mathbf{z})$ and \mathbf{s} and then apply ADMM. Since \mathcal{L} is separable with respect to the respective variables $\mathbf{x}, \mathbf{y}, \mathbf{z}$, we can further obtain the following form with four subproblems

btain the following form with four subproblems
$$\begin{cases}
\mathbf{s} \leftarrow \underset{\mathbf{s}}{\operatorname{argmin}} \frac{\rho_{1}}{2} \|\mathbf{s} - B\mathbf{x} + \widehat{\mathbf{x}}\|_{2}^{2} + \frac{\rho_{2}}{2} \|\mathbf{y} - K\mathbf{s} + \mathbf{e}_{d} + \widehat{\mathbf{y}}\|_{2}^{2} + \frac{\rho_{3}}{2} \|\mathbf{z} - \mathbf{s} + \widehat{\mathbf{z}}\|_{2}^{2} + \iota_{C_{1}}(\mathbf{s}) \\
\mathbf{x} \leftarrow \underset{\mathbf{x}}{\operatorname{argmin}} \frac{\rho_{1}}{2} \|\mathbf{s} - B\mathbf{x} + \widehat{\mathbf{x}}\|_{2}^{2} \\
\mathbf{y} \leftarrow \underset{\mathbf{x}}{\operatorname{argmin}} \|\mathbf{y}\|_{1} + \frac{\rho_{2}}{2} \|\mathbf{y} - K\mathbf{s} + \mathbf{e}_{d} + \widehat{\mathbf{y}}\|_{2}^{2} \\
\mathbf{z} \leftarrow \underset{\mathbf{z}}{\operatorname{argmin}} \frac{\rho_{3}}{2} \|\mathbf{z} - \mathbf{s} + \widehat{\mathbf{z}}\|_{2}^{2} + \iota_{C_{2}}(\mathbf{z}) \\
\widehat{\mathbf{x}} \leftarrow \widehat{\mathbf{x}} + \mathbf{s} - B\mathbf{x} \\
\widehat{\mathbf{y}} \leftarrow \widehat{\mathbf{y}} + \mathbf{y} - K\mathbf{s} + \mathbf{e}_{d} \\
\widehat{\mathbf{z}} \leftarrow \widehat{\mathbf{z}} + \mathbf{z} - \mathbf{s}
\end{cases}$$

The parameters ρ_1 , ρ_2 , ρ_3 are all positive real numbers. Note that the parameters ρ_1 and ρ_3 can be skipped in the respective **x**-subproblem and **z**-subproblem since scaling of the objective function in an optimization problem makes no impact on the solution. Firstly, the **s**-subproblem has a least-squares solution restricted to the set C_1

$$\mathbf{s} \leftarrow \operatorname{proj}_{C_1}(\rho_1 I_n + \rho_2 K^T K + \rho_3 I_n)^{-1} \left(\rho_1 (B\mathbf{x} - \widehat{\mathbf{x}}) + \rho_2 K^T (\mathbf{y} + \mathbf{e}_d + \widehat{\mathbf{y}}) + \rho_3 (\mathbf{z} + \widehat{\mathbf{z}})\right). \tag{5}$$

Here the projection operator $\operatorname{proj}_{C_1}(\cdot)$ is essentially the projection onto the ℓ_{∞} -ball defined componentwise by $\left(\operatorname{proj}_{\|\cdot\|_{\infty}\leq c}(\mathbf{x})\right)_i = \min(c, \max(-c, x_i))$. In fact, the number of parameters in the s-subproblem can be reduced to two after scaling. Similarly, the **x**-subproblem has a least-squares solution

$$\mathbf{x} \leftarrow (B^T B)^{-1} B^T (\mathbf{s} + \widehat{\mathbf{x}}). \tag{6}$$

Next, the y-subproblem has a closed-form solution

$$\mathbf{y} \leftarrow \operatorname{shrink}(K\mathbf{s} - \mathbf{e}_d - \widehat{\mathbf{y}}, 1/\rho_2).$$
 (7)

Here the shrinkage operator (a.k.a. the proximal operator of ℓ_1 -norm) shrink (\cdot, \cdot) is defined componentwise by $\left(\operatorname{shrink}(\mathbf{x}, \sigma)\right)_i = \operatorname{sign}(x_i) \max(|x_i| - \sigma, 0)$. Lastly, similar to the **s**-subproblem, the **z**-subproblem has a least-squares solution restricted to the set C_2 and thus

$$\mathbf{z} \leftarrow \operatorname{proj}_{C_2}(\mathbf{s} - \widehat{\mathbf{z}}).$$
 (8)

Similar to $\operatorname{proj}_{C_1}(\cdot)$, the operator $\operatorname{proj}_{C_2}(\cdot)$ is the projection onto the ℓ_1 -ball defined by

 $\operatorname{proj}_{\|\cdot\|_1 \le c}(\mathbf{x}) = \begin{cases} \mathbf{x}, & \text{if } \|\mathbf{x}\|_1 \le c, \\ \frac{c\mathbf{x}}{\|\mathbf{x}\|_1}, & \text{if } \|\mathbf{x}\|_1 > c. \end{cases}$

Similar to [2], it can be shown that the proposed algorithm converges to the solution of (3) with convergence rate O(1/k) where k is the iteration number.

3 Experimental Results

3.1 Experimental Design

The computational experiments are designed to compare the performance of several methods, including the conventional two pad electrodes, the constrained least squares (CLS) method, LCMV, maximum intensity (MI) method and the proposed one. In the experiments, we choose two different anatomical target types: single target and multiple targets. The single target contains only one active voxel in the motor cortex, shown in Fig. 2(a). The desired intensity is set to be 0.3 V/m [12]. This single target experiment aims to simulate the performance when algorithms are applied to the common clinical use. The test multiple targets are acquired from the results of the EEG source localization, shown in Fig. 3(a). The desired maximum intensity \mathbf{e}_o restricted on those three target regions are 0.3727 V/m, 0.3522 V/m and 0.2841 V/m, respectively. The multiple-target experiment can help exam the performance of EEG-guided brain stimulation. In both experiments, we fix $I_{\text{max}} = 2$ mA and $I_{total} = 4$ mA.

3.2 Comparison Metrics

To make comparison fair and comprehensive, we use three quantitative evaluation criteria, i.e., the stimulation precision, accuracy and intensity. Similar to the existing studies, we measure the stimulation precision (focality) by calculating the "half-max radius" [5] with a unit of millimeter (mm). By default, all length units are the millimeter. The difference is that we define $\mathbf{r}_{0.5} = \mathbf{r}|_{E(\mathbf{r})=0.5}$ to be the radius that contains half of the total energy. Here the portion of the energy contained within a circle of increasing radius around the mass center, denoted by $E(\mathbf{r})$, is defined by

$$E(\mathbf{r}) = \frac{\sum_{i \in \Gamma(\mathbf{r})} \|\mathbf{e}(\mathbf{r}_i)\|_2^2}{\sum_i \|\mathbf{e}(\mathbf{r}_i)\|_2^2},$$

where the $\Gamma(\mathbf{r})$ is the set containing all the voxels that lie within a distance of \mathbf{r} from the center of the target region. Higher value of $\mathbf{r}_{0.5}$ indicates the more spread-out e-field distribution, while lower $\mathbf{r}_{0.5}$ suggests a better focality case that most of the energy are concentrated in a small region and it has better focusing capability. Target Error (TE) is the second criterion which is designed to evaluate the stimulation accuracy. The first and second metrics are the mass center of the target region and the activation region. Next, we define the third metric to assess the TE, which is the Euclidean distance between these two mass centers, i.e.,

$$TE = \|MC_0 - MC\|_2, \quad MC_{j0} = \frac{\sum_i \mathbf{e}_0(\mathbf{r}_i)_j \cdot \mathbf{r}_{ij}}{\sum_i \mathbf{r}_{ij}}, \quad MC_j = \frac{\sum_i \mathbf{e}(\mathbf{r}_i)_j \cdot \mathbf{r}_{ij}}{\sum_i \mathbf{r}_{ij}},$$

for $j \in \{x, y, z\}$. The last criterion is the intensity of the target region in V/m. If the target region contains more than one voxel, we will compare both the average intensity and the maximum intensity of the target region. According to the literature and clinical records, tDCS will be efficient enough when the produced intensity is about $0.2 \text{ V/m} \sim 0.3 \text{ V/m}$ at the target region [12]. In addition, clinical application favors the result that is close to the desired e-field distribution in the target region. Note that we evaluate the performance of each target region separately if we stimulate the multiple targets at the same time.

3.3 Results

In the single target study, we first simulated the e-field distribution produced by the conventional electrode configuration (CEC). From the Fig. 2, one can see that this conventional montage will cause an effect on not only the motor cortex region, but also the other regions nearby, like the auditory cortex. Here we skip LCMV for comparison due to its failure to produce feasible results under the total current constraints. MI sacrifices even more focality to produce higher e-field intensity at the target area. On the contrary, CLS reduces the intensity to achieve better stimulation accuracy and precision. However, it is about two orders of magnitude less than the conventional system, which is not sufficient for the clinical treatment. The proposed result with $\rho_1 = 1$, $\rho_2 = 5$, and $\rho_3 = 4$ maintains a good balance among intensity, accuracy and precision, shown in Fig. 2. By enlarging the value of ρ_3 , we can get a much more focal and accurate stimulation while maintaining the sufficient intensity with fewer iterations. Quantitative evaluation results are shown in the Table 1.

For the multiple targets study, conventional electrode is no longer applicable. Moreover, for this complicated stimulation pattern, LCMV has no feasible solution due to its strict constraints as we discussed in Sect. 1. Therefore, we can only compare the results of the constrained least squares, maximum intensity and proposed method with $\rho_1 = 10$, $\rho_2 = 10^{-2}$, and $\rho_3 = 10^{-1}$. The e-field distribution patterns are shown in the Fig. 3, and detailed quantitative evaluations are shown in the Table 2. The maximum intensity method, as expected, produces the highest intensity among the all methods being compared. However, it influences

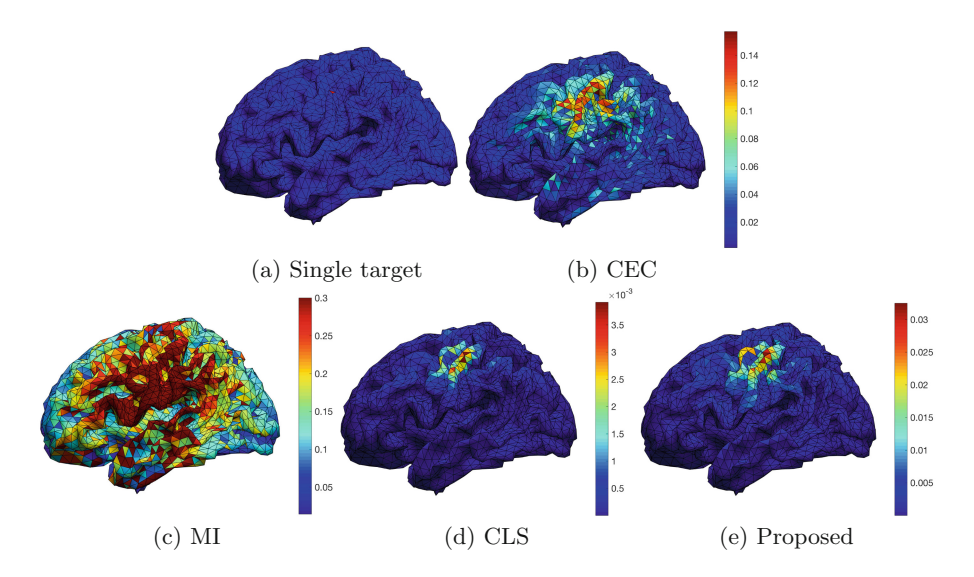


Fig. 2. E-field distribution patterns for the single-target case.

Table 1. Quantitative evaluation comparison of various single-target results with the desired e-field distribution at the target $\|\mathbf{e}_o\|_2 = 0.3$.

	Intensity	Focality	TE
CEC	0.1571	61.6189	13.8624
MI	1.4572	69.5048	27.1784
CLS	0.0039	17.5171	2.0436
Proposed	0.0325	18.5877	5.9834

the entire left side cortex and has the largest target errors in all three target regions. The constrained least squares method mimics the desired electric field distribution pattern, but the intensity is almost an order of magnitude less than the desired intensity, which is not sufficient for real applications. We also include the results obtained by applying the proposed method with two different sets of parameters ρ_1, ρ_2, ρ_3 . The first result with $\rho_1 = 10, \rho_2 = 10^{-2}, \rho_3 = 10^{-1}$ (see Fig. 3(d)) is similar to the constrained least squares one that can successfully produce the desired pattern and has small target errors in all three target regions, but the intensity is not strong enough. The second result with $\rho_1 = 10, \rho_2 = \rho_3 = 10^6$ (see Fig. 3(e)), which is less focal compared to the first pattern, achieves the higher intensity that is more appropriate for clinical applications than the other results. In the meanwhile, it still has small target errors and the focality is much better than the maximum intensity method. Overall, the proposed method can achieve a well-balanced result with high intensity, accuracy, and focality.

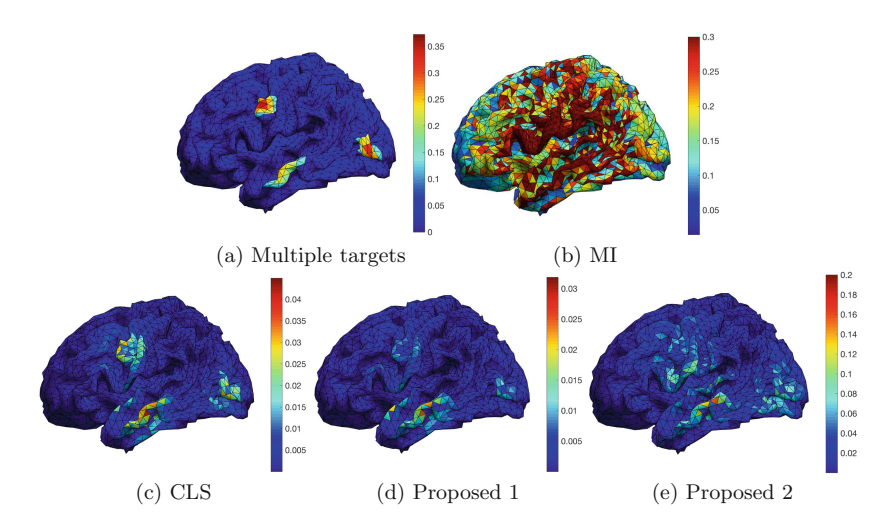


Fig. 3. E-field distribution patterns for the multiple-target case.

Table 2. Quantitative evaluation comparison of various multiple-target results. The desired e-field distribution at the three targets are 0.3727 V/m, 0.3522 V/m, and 0.2841 V/m, respectively.

	Intensity			Focality			TE		
MI	0.6032	0.3880	0.8406	57.0119	91.6543	46.8141	25.4935	27.2086	14.9702
CLS	0.0303	0.0297	0.0449	15.7622	14.8578	20.1903	10.7691	4.1970	4.7183
Proposed 1	0.0111	0.0125	0.0281	31.8789	13.1003	27.5492	11.6089	5.8121	3.3800
Proposed 2	0.0648	0.0876	0.1493	31.1384	23.7444	24.5476	12.7423	9.6420	6.2396

From the two experiments above, one can see several advantages of the proposed method over the state-of-the-art methods. First, the proposed method provides flexibility to achieve different desirable results by adjusting the values of ρ_1, ρ_2, ρ_3 within a limited number of iterations. The penalty parameters ρ_1, ρ_2, ρ_3 play an important role in balancing the trade-off between the intensity and the stimulation accuracy/precision at each iteration. As a matter of fact, another related method-weighted least squares (WLS)-has been proposed in [5]. However, WLS is complicated for implementation, since it requires the intervene of a clinician to specify the weight of the error term at each voxel. Moreover, the WLS results can not be directly predicted by the weighting parameters, which also makes it time consuming. By contrast, the proposed method can produce various favorable e-field distribution patterns easily. Second, the proposed method can produce effective stimulation pattern with reasonable stimulation accuracy and precision. Last but not least, the proposed method has empirically been shown to provide minimum error solutions with high accuracy and focality for clinical applications.

4 Conclusions

In this work, we propose a practically useful multi-electrode tDCS configuration model with the ℓ_1 -norm fidelity and multiple constraints due to the safety consideration. To handle the non-differentiability of the objective function in the model, we rewrite the problem by the change of variables and then apply ADMM to derive an efficient numerical algorithm. Simulation experiments have demonstrated the flexibility of this method, i.e., yielding different desirable stimulation patterns by varying the parameters. By qualitatively and quantitatively comparing with other state-of-the-art methods, the proposed method has shown the great potential in providing optimal results with high accuracy and focality.

Acknowledgments. The research of Jing Qin is supported by the NSF grant DMS-1818374.

References

- Auvichayapat, N., et al.: Transcranial direct current stimulation for treatment of refractory childhood focal epilepsy. Brain Stimul.: Basic Transl. Clin. Res. Neuromodul. 6(4), 696-700 (2013)
- Boyd, S., Parikh, N., Chu, E., Peleato, B., Eckstein, J.: Distributed optimization and statistical learning via the alternating direction method of multipliers. Found. Trends® Mach. Learn. 3(1), 1–122 (2011)
- Brunoni, A.R., et al.: The escitalopram versus electric current therapy for treating depression clinical study (ELECT-TDCS): rationale and study design of a noninferiority, triple-arm, placebo-controlled clinical trial. São Paulo Med. J. 133(3), 252-263 (2015)
- Chan, T.F., Esedoglu, S.: Aspects of total variation regularized l₁ function approximation. SIAM J. Appl. Math. 65(5), 1817–1837 (2005)
- Dmochowski, J.P., Datta, A., Bikson, M., Su, Y., Parra, L.C.: Optimized multielectrode stimulation increases focality and intensity at target. J. Neural Eng. 8(4), 046011 (2011)
- Fregni, F., et al.: Noninvasive cortical stimulation with transcranial direct current stimulation in parkinson's disease. Mov. Disord. 21(10), 1693–1702 (2006)
- Gabay, D., Mercier, B.: A dual algorithm for the solution of nonlinear variational problems via finite element approximations. Comput. Math. Appl. 2, 17–40 (1976)
- 8. Glowinski, R., Marrocco, A.: Sur l'approximation, par elements finis d'ordre un, et la resolution, par, penalisation-dualité, d'une classe de problems de dirichlet non lineares. Revue Française d'Automatique, Informatique, et Recherche Opéationelle 9, 41–76 (1975)
- 9. Guler, S.: Optimization of focality and direction in dense electrode array transcranial direct current stimulation (tDCS). J. Neural Eng. 13(3), 036020 (2016)
- Li, F., Osher, S., Qin, J., Yan, M.: A multiphase image segmentation based on fuzzy membership functions and L1-norm fidelity. J. Sci. Comput. 69(1), 82–106 (2016)
- 11. Oostenveld, R., Fries, P., Maris, E., Schoffelen, J.M.: FieldTrip: open source software for advanced analysis of MEG, EEG, and invasive electrophysiological data. Comput. Intell. Neurosci. **2011**, 1 (2011)

- 12. Ruffini, G., Fox, M.D., Ripolles, O., Miranda, P.C., Pascual-Leone, A.: Optimization of multifocal transcranial current stimulation for weighted cortical pattern targeting from realistic modeling of electric fields. Neuroimage 89, 216–225 (2014)
- 13. Sadleir, R., Vannorsdall, T.D., Schretlen, D.J., Gordon, B.: Target optimization in transcranial direct current stimulation. Front. Psychiatry 3, 90 (2012)
- 14. Woods, A.J., et al.: A technical guide to tDCS, and related non-invasive brain stimulation tools. Clin. Neurophysiol. **127**(2), 1031–1048 (2016)